

Grid Generation for General Three-Dimensional Configurations

K. D. Lee, M. Huang, N. J. Yu and P. E. Rubbert
 The Boeing Company
 Seattle, Washington

Abstract

The objective of the present study is to construct a suitable grid system for complex 3-D configurations such as a wing/body/nacelle shape for the solution of nonlinear transonic flow problems. Two approaches have been explored based on Thompson's body-fitted coordinate concept. The most general approach is to divide the computational domain into multiple rectangular blocks where the configuration itself is also represented by a set of blocks, whose structure follows the natural lines of the configuration. The block-structured grid system is adaptable to complex configurations and gives good grid quality near physical corners. However, it introduces algorithm issues for the flow solution concerning the treatment of nonanalytic grid block boundaries and nonstandard grid cells. These issues have been explored in relation to the grid generation. A more limited approach treats a wing/body configuration with only a single rectangular block in computational space. In this treatment the issues involving nonstandard cells are avoided, but other limitations on grid resolution appear. Both a linear and a nonlinear system of grid generation equations have been developed including methods of grid control. The linear method can generate grids of comparable quality with order-of-magnitude less cost. Its disadvantage is the greater possibility of ill-conditioned grids which, however, can be easily controlled in the block-structured grid system.

Grid Generation Equations

1 Linear System

$$\vec{x}_{\xi\xi} + B\vec{x}_{\eta\eta} + C\vec{x}_{\zeta\zeta} + D\vec{x}_{\xi} + E\vec{x}_{\eta} + F\vec{x}_{\zeta} + G = 0$$

$$\vec{x} = (x, y, z)$$

B to G: grid control functions of $\xi, \eta,$ and/or ζ

2 Nonlinear System

$$A\left(\vec{x}_{\xi\xi} + \frac{P}{J^2-A}\vec{x}_{\xi}\right) + B\left(\vec{x}_{\eta\eta} + \frac{Q}{J^2-B}\vec{x}_{\eta}\right) + C\left(\vec{x}_{\zeta\zeta} + \frac{R}{J^2-C}\vec{x}_{\zeta}\right) + 2\left(D\vec{x}_{\xi\eta} + E\vec{x}_{\xi\zeta} + F\vec{x}_{\eta\zeta}\right) = 0$$

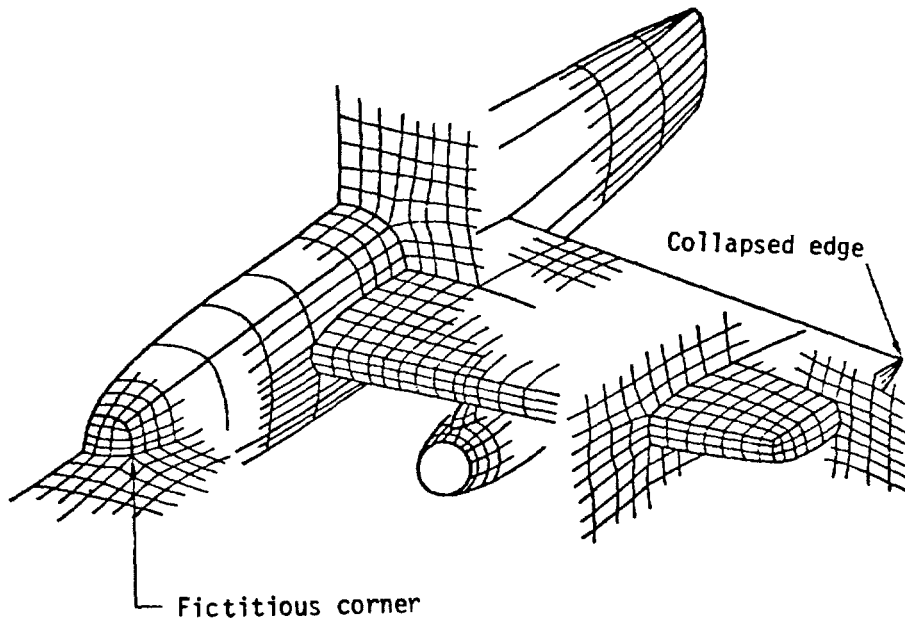
A to F: coupling terms functions of x, y, and z

P, Q, R: grid control

J = Jacobian of the transformation

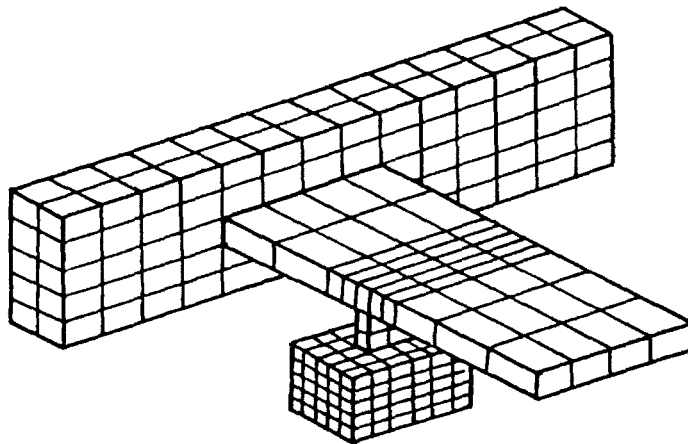
Figure 1. Block structuring

This is a schematic illustration of a typical block structured grid about a wing/body/nacelle configuration. The multi-block grid obviously provides more desirable grid densities and eliminates the "lost corner." However, it introduces special points termed a "fictitious corner," a "collapsed edge," and a nonanalytic block boundary.



Physical space

ORIGINAL PAGE IS
OF POOR QUALITY



Computational space

Figure 2. Comparison of grid structure

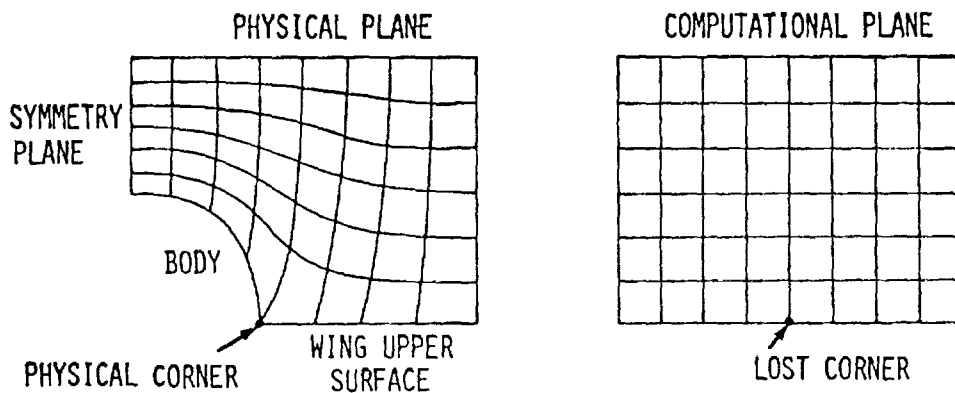
Lost corner - a physical corner transformed into a smooth point in the computational space

Fictitious corner - a smooth point transformed into a corner point in the computational space

Nonanalytic block boundary - grid lines across the block boundary are continuous but not smooth

Collapsed edge (3-D) - grid lines merge together in the physical space

(A) SINGLE-BLOCK GRID



(B) MULTIPLE-BLOCK GRID

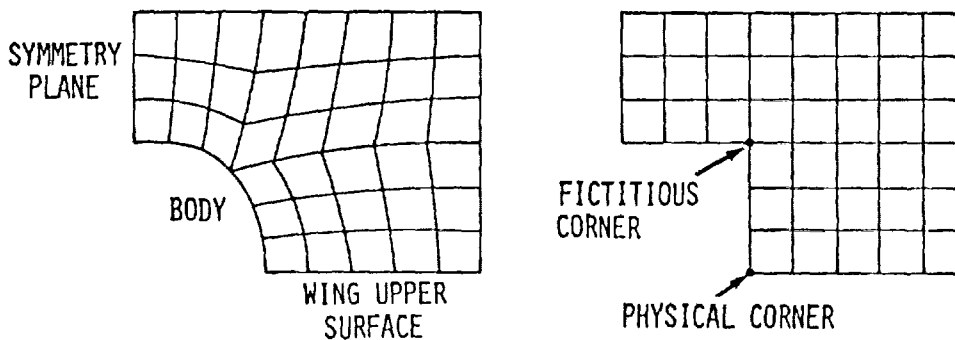


Figure 3. Block-structured grid generation process

After defining the overall block structure, a one-dimensional grid generation along the block perimeters produces a perimeter discretization. This provides boundary conditions for a subsequent two-dimensional grid generation producing grids covering the block surfaces. These in turn serve as boundary conditions to produce three-dimensional volume grids filling each block.

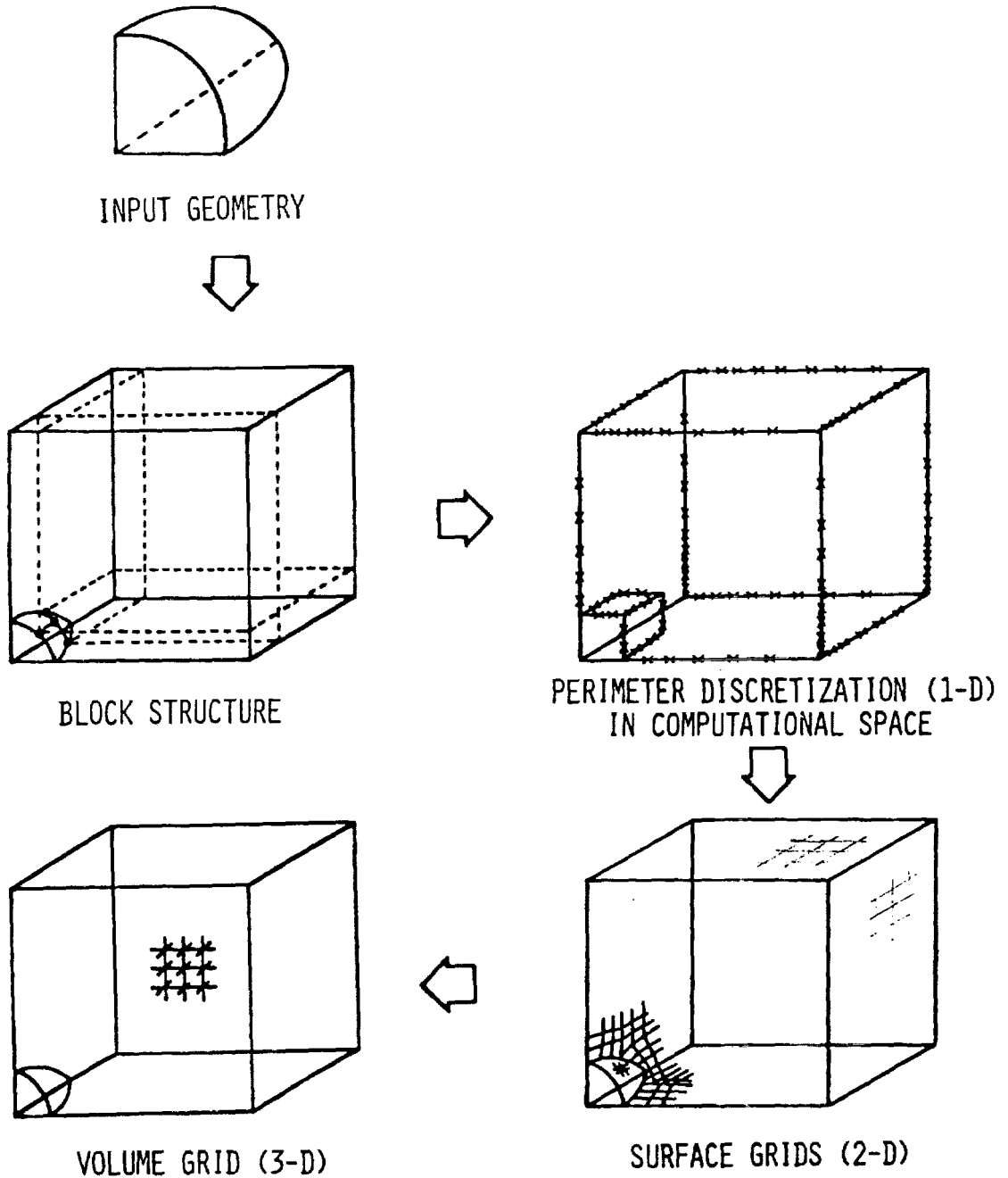
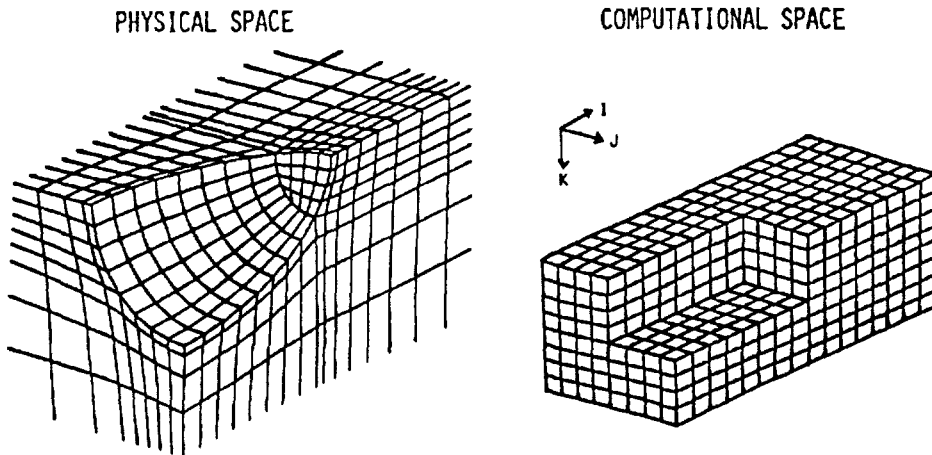


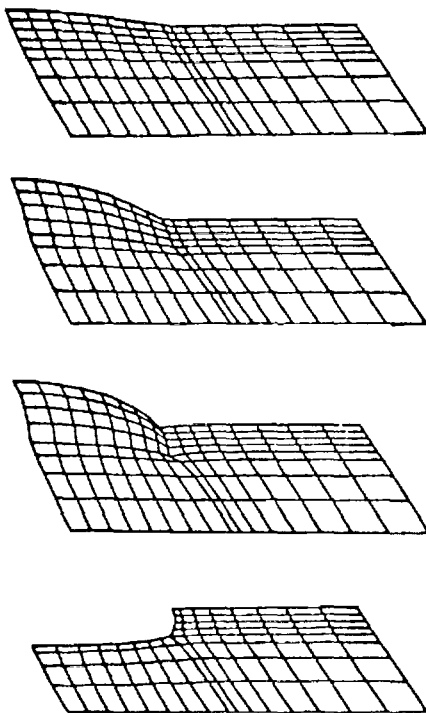
Figure 4. Block-structure grid for an ellipsoid

This example shows the grid around an ellipsoid which has been transformed to a cube in computational space. Fictitious corners can be seen.

(A) ON THE BOUNDARY SURFACE



(B) VOLUME GRIDS: $K = \text{CONSTANT}$



(C) VOLUME GRIDS: $I = \text{CONSTANT}$

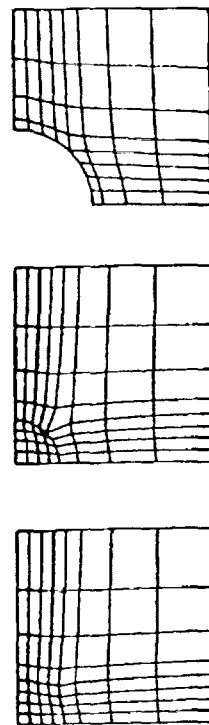


Figure 5. Algorithm compatability study

The effect of the grid structure and the special points on the flow solution is explored by solving the potential flow over a cylinder. Cell-oriented flux formulation is used to treat the algorithm issues. Surprisingly, all the grid systems yield good resolution. Accuracy depends on the cell size rather than the grid structure at the special points.

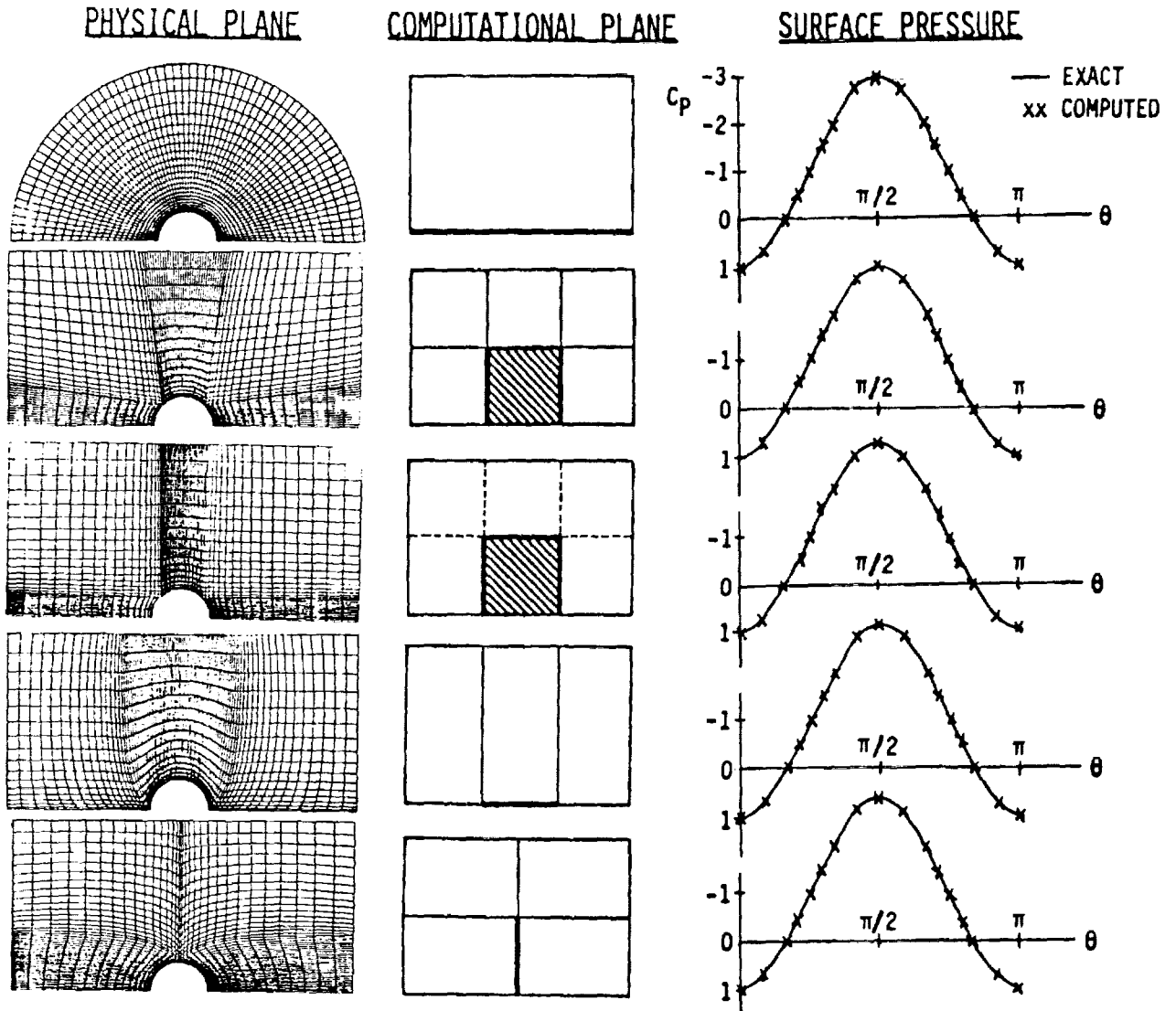
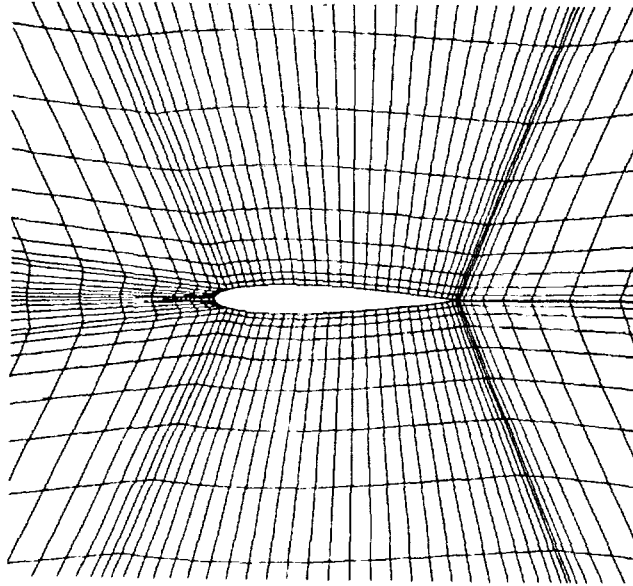


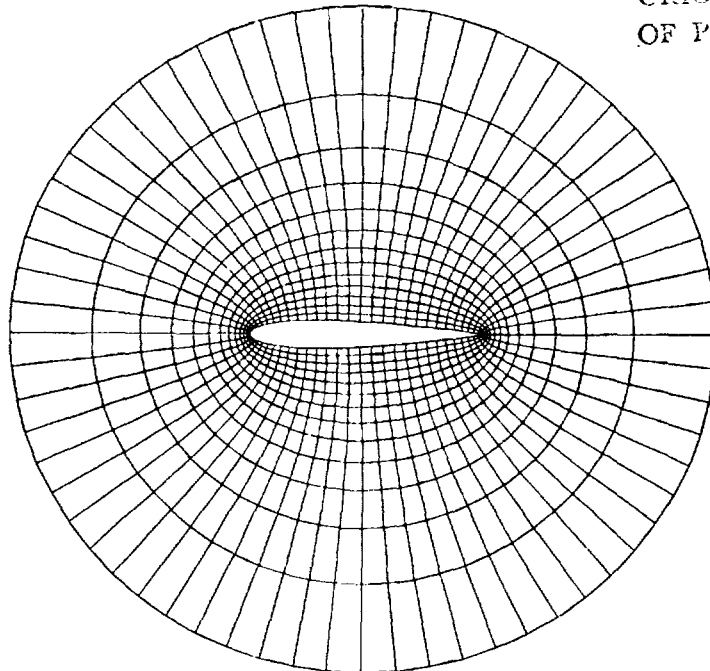
Figure 6. Comparison of grids near an airfoil

The use of multi-block grid is considered for an airfoil. Compared to the ring-type grid, the multi-block grid seems to be overly complex. Its advantage is in its adaptability to more complex geometry.

MULTIPLE-BLOCK GRID



SINGLE-BLOCK GRID



ORIGINAL DRAWING
OF POOR QUALITY

Figure 7. Airfoil study

The ability to produce accurate solutions using the multi-block grid is demonstrated in subsonic and transonic regions. Compared to the results from the ring-type single-block grid, remarkable accuracy was obtained even when the fictitious corner is located in supersonic regions. All the flow and metric quantities are defined at the center of each cell and the artificial density method is adopted for the density retardation in supersonic region.

PRESSURE DISTRIBUTION (NACA 0012 AIRFOIL)

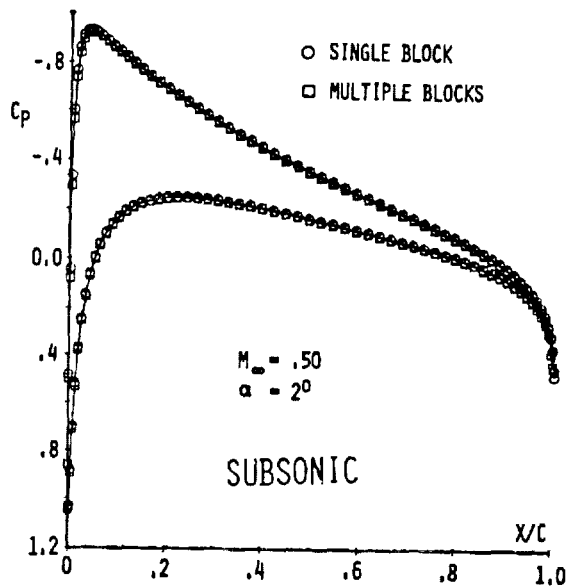
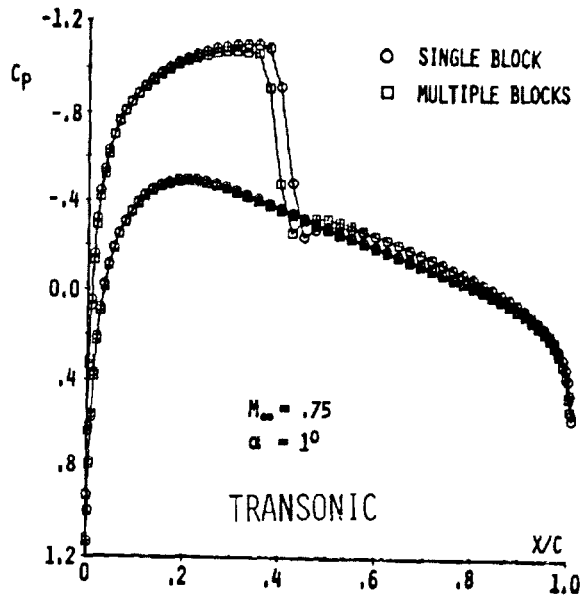


Figure 8. Surface grid for a wing/body
(single-block structure)

The use of the C-type grid provides smooth grid distribution near the wing leading edge. The body surface line on the symmetry plane coincides with a grid line which consists of lost corners. One concern is grid quality at the wing tip.

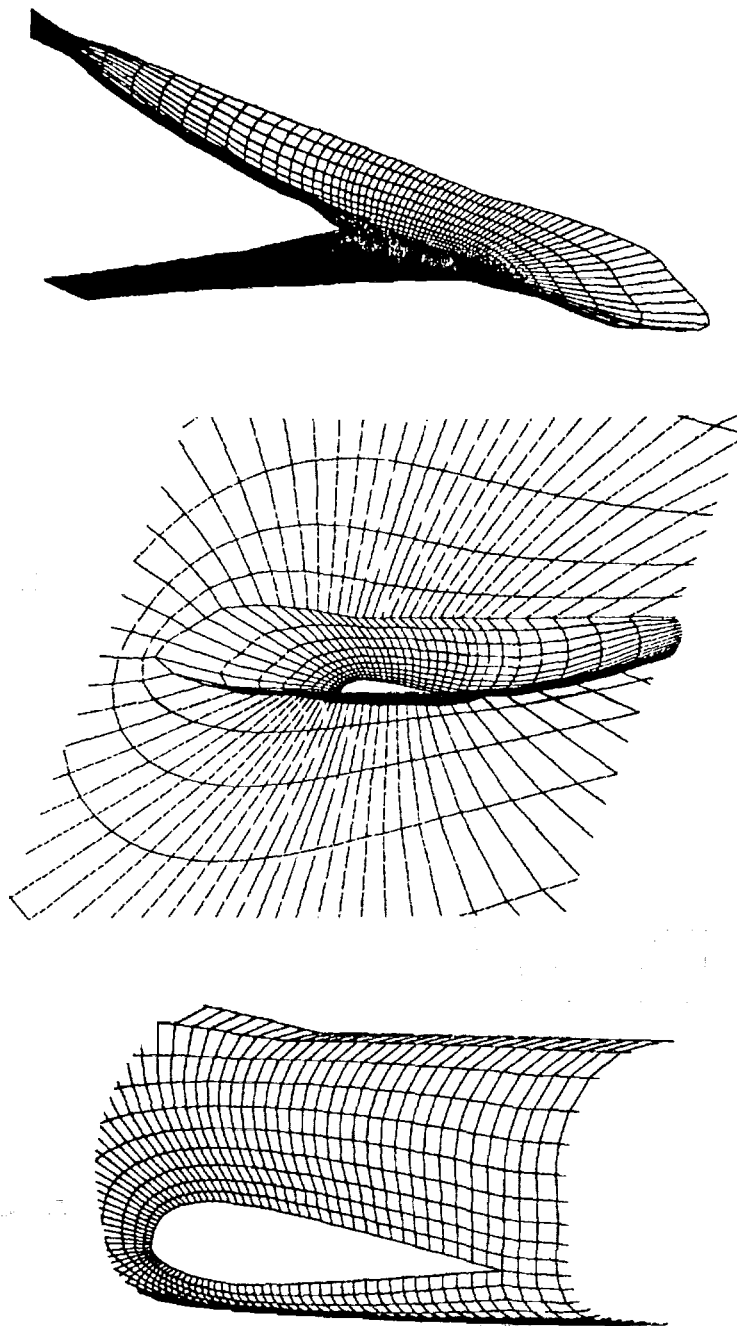


Figure 9. Surface grid for a wing/body
(multi-block structure)

The use of a multi-block grid eliminates the lost corners in the single-block grid of figure 8 and improves the grid quality near the wing tip, while producing the fictitious corners and nonanalytic block boundaries. Its ability to extend to more complex configurations is obvious.

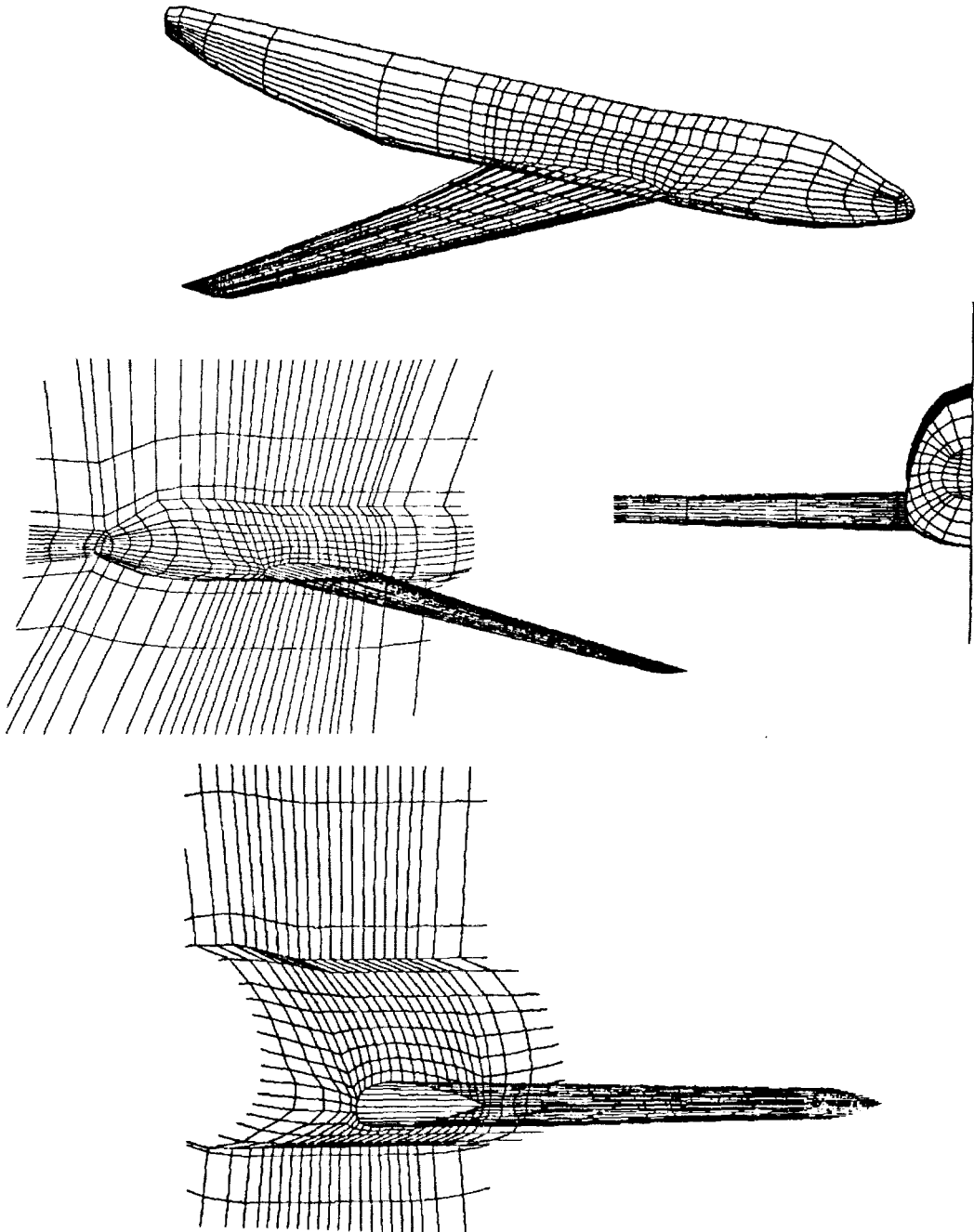
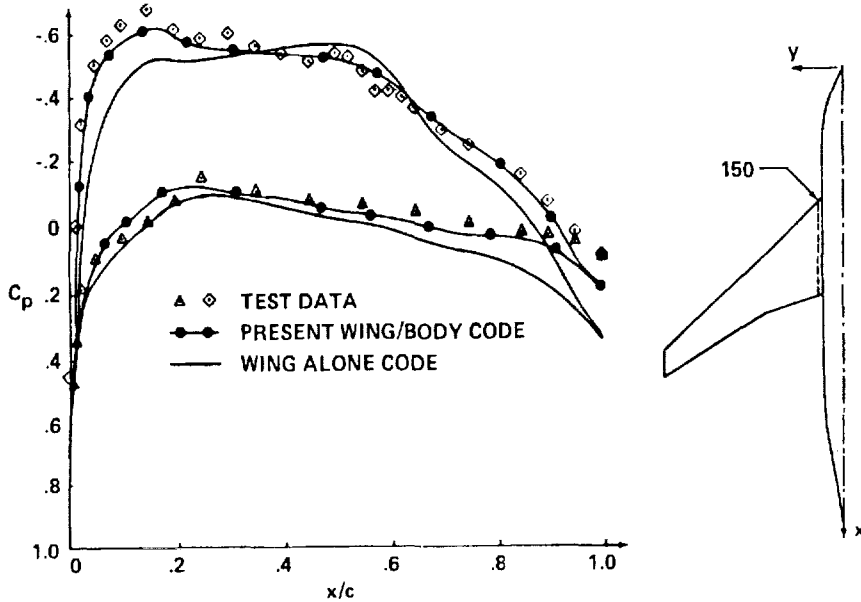


Figure 10. 3-D flow solution

A transonic solution for a wing/body combination is obtained using the single-block grid and compared to the experimental results. The use of body-fitted grid system improves the accuracy near the wing/body junction.

LOW WING CONFIGURATION AT $M_\infty = .84, \alpha = 2.8^\circ$



STATION $y = 495$

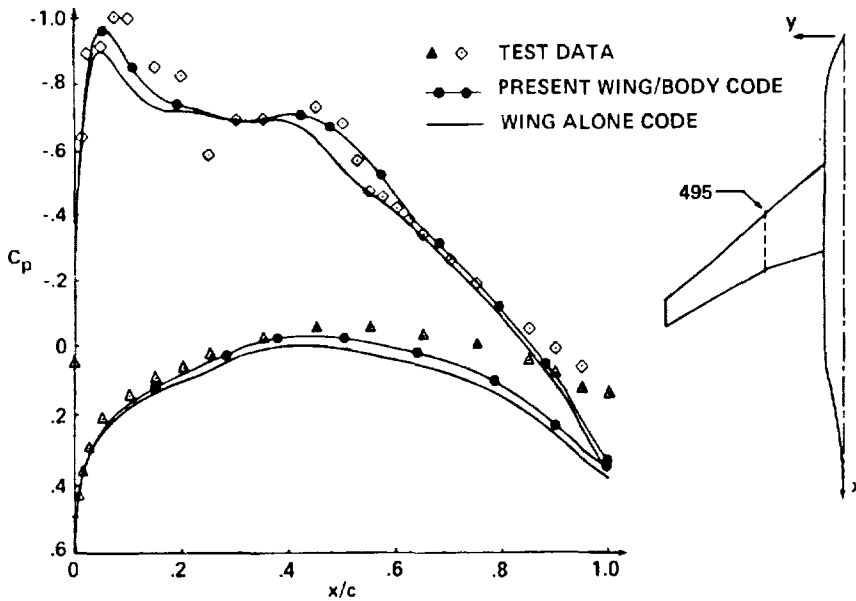
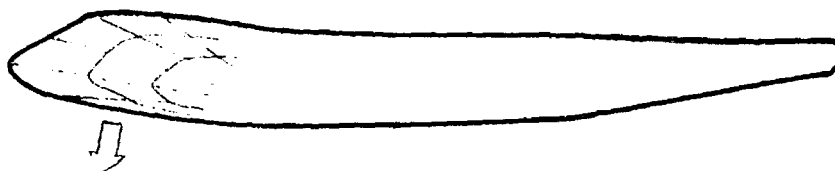


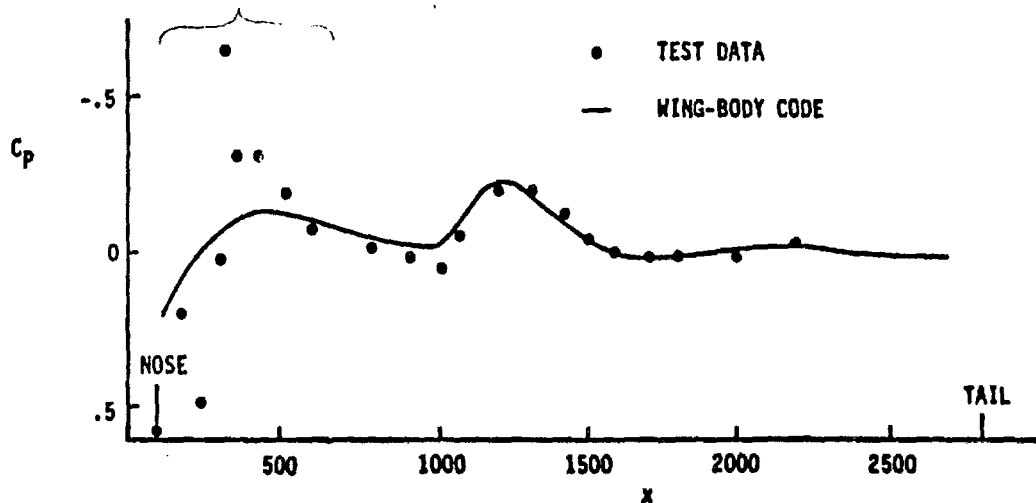
Figure 11. 3-D flow solution

The body-fitted grid system can produce quite accurate pressure distribution even on the body surface. Very coarse nose grid distribution prevents fine pressure resolution in that region.

CROWN LINE PRESSURES FOR 747-200
AT $M_\infty = .84$, $\alpha = 2.8^\circ$



VERY COARSE NOSE GRIDS PREVENT FINE PRESSURE RESOLUTION



ORIGINAL PAGE IS
OF POOR QUALITY